

Temperature dependence of binary and ternary recombination of H_3^+ ions with electrons

J. Glosík, R. Plašil, I. Korolov, T. Kotřík, O. Novotný, P. Hlavenka, P. Dohnal, and J. Varju
Charles University, Mathematics and Physics Faculty, Prague 8, Czech Republic

V. Kokoouline

Department of Physics, University of Central Florida, Orlando, Florida 32816, USA

Chris H. Greene

Department of Physics and JILA, University of Colorado, Boulder, Colorado 80309-0440, USA

(Dated: October 23, 2018)

We study binary and the recently discovered process of ternary He-assisted recombination of H_3^+ ions with electrons in a low temperature afterglow plasma. The experiments are carried out over a broad range of pressures and temperatures of an afterglow plasma in a helium buffer gas. Binary and He-assisted ternary recombination are observed and the corresponding recombination rate coefficients are extracted for temperatures from 77 K to 330 K. We describe the observed ternary recombination as a two-step mechanism: First, a rotationally-excited long-lived neutral molecule H_3^* is formed in electron- H_3^+ collisions. Second, the H_3^* molecule collides with a helium atom that leads to the formation of a very long-lived Rydberg state with high orbital momentum. We present calculations of the lifetimes of H_3^* and of the ternary recombination rate coefficients for para and ortho- H_3^+ . The calculations show a large difference between the ternary recombination rate coefficients of ortho and para- H_3^+ at temperatures below 300 K. The measured binary and ternary rate coefficients are in reasonable agreement with the calculated values.

I. INTRODUCTION

Electron scattering by the simplest polyatomic ion H_3^+ is of fundamental importance in plasma physics because H_3^+ ions are dominant in many hydrogen-containing plasmas, including astrophysically-relevant plasmas in particular. For quantum theory, the electron- H_3^+ interaction is important because the process involves the simplest polyatomic ion that can be studied from first principles without adjustable parameters. In the long history of research on recombination of H_3^+ with an electron there have been numerous exciting, contradictory and sometimes unaccepted results. We mention here only a few recent reviews devoted to H_3^+ recombination at low temperatures (see e.g. [1, 2, 3, 4, 5]). A successful theory of H_3^+ recombination with electrons at scattering energies below 1 eV was developed relatively recently when the Jahn-Teller non-Born-Oppenheimer coupling was included into theory [6, 7, 8, 9]. The measurements of the recombination rate constant in different storage ring experiments have also converged to the same value recently, after it became understood that the internal rotational and vibrational degrees of freedom of the H_3^+ ion influence the recombination rate [8, 10, 11]. The theoretical developments and improvements in storage ring experiments have resulted in a reconciliation of theory and experiment for the binary electron- H_3^+ recombination process.

However, the H_3^+ and D_3^+ recombination experiments carried out in afterglow plasmas [3, 4, 5, 12, 13, 14, 15, 16, 17] have repeatedly given rate coefficients very different from the ones obtained in the aforementioned storage ring experiments and the theoretical calculations. Until now, the plasma studies have not been fully understood

and, as a result, they have been frequently rejected because they do not mesh with the present understanding of the binary DR process (see, e.g., the very recent review discussing this subject [18]). However, the experimental plasma results are reproducible and they demand an understanding and an integration into the full picture of H_3^+ recombination with electrons. The present work discusses and, we hope, clarifies some aspects of this complex problem.

The plasma measurements are usually carried out in a He/Ar/ H_2 gas mixture (see the review by Plašil *et al.* [3]) or in a pure H_2 gas [14, 19]. The main question is how to “reconcile” [16] the rate constant (including its dependence on experimental conditions) observed in an H_3^+ dominated plasma with actual theory and with data from the storage ring experiments [18]. The plasma experiments are typically carried out with helium buffer gas at pressures in the range 50–2000 Pa. It has been generally accepted that such pressures are too small to produce appreciable ternary helium-assisted recombination of H_3^+ . The fact that the neutral-stabilized recombination can sometimes play a role was predicted many years ago by Bates and Khare [20] and confirmed for some ions (but not for H_3^+) by experiments [21, 22]. The typical value for the three-body recombination rate coefficient K_{He} with helium as an ambient gas obtained in experiment and estimated theoretically [21, 22] is of order of $10^{-27} \text{ cm}^6\text{s}^{-1}$ at 300 K. Thus, at pressures of 1300 Pa, the corresponding apparent binary recombination rate coefficient is smaller than $10^{-9} \text{ cm}^3\text{s}^{-1}$, which would therefore be negligible in comparison with the now-accepted binary H_3^+ recombination rate coefficient [8, 9, 10, 11, 18]. This would also be negligible in comparison with the bi-

nary rate coefficients (about $10^{-7} \text{ cm}^3\text{s}^{-1}$ at 300 K) for the majority of molecular ions. This is the reason why the ternary recombination of H_3^+ had previously been neglected in FALP (flowing afterglow) and SA (stationary afterglow) experiments carried out at 50–2000 Pa.

In our recent study [23] we have shown that at 260 K a significant fraction of the $\text{H}_3^+ + e^-$ collisions leads to formation of long-lived (up to tens of picoseconds) rotationally-excited neutral Rydberg molecules H_3^* . The formation of long-lived H_3^* and collisions of H_3^* with helium atoms can influence the overall process of recombination of the H_3^+ dominated afterglow plasma. By measuring the helium pressure dependence of the H_3^+ recombination rate coefficient we have found that at 260 K the ternary recombination rate is comparable with the binary rate, already at pressures of several hundred Pa. The observed ternary recombination of H_3^+ ions is more efficient by a factor of 100 than the ternary recombination rate predicted by Bates and Khare [20]. This suggests that ternary recombination of H_3^+ ions is associated with intrinsic features of the interaction between H_3^+ and electrons at low collision energies [23]. The recombination process described by Bates [20] is a ternary process of a different nature.

This study presents a further extension of our measurements to a broader range of temperatures and it extracts the temperature dependence of the binary and ternary recombination rate coefficients of H_3^+ ions. Before presenting these new results and their interpretation, some of us (the Prague group) wish to provide a few comments concerning the plasma experiments made in Prague in recent years.

Previously, we have studied the H_3^+ recombination in decaying plasmas formed from a He/Ar/ H_2 gas mixture using several afterglow experiments based on several modifications of flowing and stationary afterglow apparatuses (FALP [24], AISA–Advanced Integrated Stationary Afterglow [3, 13, 17], TDT-CRDS–Test Discharge Tube with Cavity Ring-Down Spectroscopy [25, 26]). We have systematically investigated the dependence of the recombination process on hydrogen partial pressure. Initially (in 2000), our intention was to explain the influence of the internal excitation of H_3^+ ions formed in a sequence of ion-molecule reactions on the measured recombination rate coefficient. Experimental conditions were such that the plasma was decaying for a long time (up to 60 ms), so the internal excitation was quenched in collisions with He and H_2 . As a rule, we skip the first 10 ms of the decay process considering it as a formation time. At low H_2 densities, $[\text{H}_2] < 10^{12} \text{ cm}^{-3}$, and helium pressures of 100–300 Pa, we have observed a decrease of the recombination rate coefficient from $\sim 10^{-7} \text{ cm}^3\text{s}^{-1}$ to $10^{-8} \text{ cm}^3\text{s}^{-1}$ when the H_2 density was decreased from $\sim 10^{12} \text{ cm}^{-3}$ to $\sim 10^{11} \text{ cm}^{-3}$. At high hydrogen densities, $[\text{H}_2] > 10^{12} \text{ cm}^{-3}$, the measured recombination rate coefficient was independent of $[\text{H}_2]$. We will consider this again below when discuss equilibrium conditions for recombining H_3^+ plasma. A similar dependence on D_2 density was observed in a D_3^+ -

dominated afterglow plasma (see e.g. [3, 17]).

In our early experimental publications [12, 27], we derived the recombination rate coefficient from experimental measurements assuming that the process is strictly binary ($\text{H}_3^+ + e^-$) at the low-pressure limit. The assumption was based on the then-existing level of knowledge about H_3^+ recombination (see the recent and older reviews in Refs. [4, 5, 14, 18, 28, 29]). However, we soon realized that the observed dependence on hydrogen density is coupled to the multistep character of the recombination process in a plasma. The theory of binary dissociative recombination of H_3^+ is more immediately applicable to the storage ring experiments. Therefore we denoted the plasma recombination rate constant as an effective deionization rate constant α_{eff} [3, 13]. Later experiments using absorption spectroscopy for ion density measurements and for the identification of the recombining ions (TDT-CRDS) [25, 26, 30] did not clarify the mechanism of recombination in an afterglow plasma.

The interpretation of data from storage ring [5, 10, 11, 31] experiments and from afterglow [3, 5, 14, 15, 16, 17, 24, 25, 32] experiments was at this point not reconciled [4, 5, 18, 33]. We stress here one principal difference between the two types of experiments: In a storage ring experiment, the recombining ions and electrons have a small adjustable relative velocity; the measured cross-section corresponds to the binary electron-ion recombination process. In a plasma experiment an ambient gas must be used. Typically, the pressure of the ambient gas in the afterglow experiments is 50–2000 Pa. The ions and electrons in afterglow plasma undergo multiple collisions with neutral particles (He and H_2 in the experiments discussed here) prior to their mutual collisions; these are collisions at low energy (around $\sim 0.025 \text{ eV}$). In a storage ring, collisions of H_3^+ with neutral particles are also possible, but when an ion collides with a background gas molecule or atom, it is removed from the beam and does not contribute any further to the observable recombination events [5].

Plasma experiments measure the thermally averaged rate constant. It means that the afterglow plasma should ideally be in thermal equilibrium with respect to all degrees of freedom, in particular with respect to the rotational, vibrational and nuclear spin states of H_3^+ . Molecular hydrogen present in the recombining plasma equilibrates the ortho/para- H_3^+ ratio and should make the “kinetic” temperature of ions and electrons to coincide with the He temperature [34, 35]. An internal excitation of H_3^+ ions obtained in the process of H_3^+ formation [3, 4] is also quenched in collisions with He atoms, but the population of the lowest energy levels (lowest ortho and para-states) is governed by collisions with H_2 . One has to have in mind that proton transfer reactions (from ArH^+ or H_2^+ to H_2) producing H_3^+ occur at nearly the rate of elastic collisions, but the rate coefficients for reactions between H_3^+ and H_2 , which change ortho- H_3^+ to para- H_3^+ and vice versa (“state changing collisions”) are a factor of 5–10 smaller, $k_{\text{sc}} \sim 3 \times 10^{-10} \text{ cm}^3\text{s}^{-1}$

(see Refs. [36, 37, 38]). If recombination of H_3^+ is sensitive to the nuclear spin state of H_3^+ then recombination drives the H_3^+ ions out of ortho/para thermal equilibrium. In contrast, the “state-changing collisions” with H_2 shift the ortho/para H_3^+ distribution towards the thermal equilibrium. In this case, thermal equilibrium means a population of rotational states corresponding to thermodynamic equilibrium at the given temperature. Note that we have already demonstrated that in a plasma at 260 K the recombination of ortho and para- H_3^+ ions is very different [23]. The recombination frequency (number of events per unit time) is $\nu_{\text{rec}} \sim \alpha_{\text{eff}} n_e$ and the “state changing frequency” is $\nu_{\text{sc}} \sim k_{\text{sc}}[\text{H}_2]$. The condition $\nu_{\text{sc}} > \nu_{\text{rec}}$ required for thermal equilibrium leads to $k_{\text{sc}}[\text{H}_2] > \alpha_{\text{eff}} n_e$. If values typical for FALP experiments ($n_e \sim 2 \times 10^9 \text{ cm}^{-3}$ and $\alpha_{\text{eff}} \sim 1.5 \times 10^{-7} \text{ cm}^3 \text{ s}^{-1}$) are used in this inequality, we obtain the condition on the hydrogen density: $[\text{H}_2] > 10^{12} \text{ cm}^{-3}$. This is an important density value for the interpretation of data in the plasma experiments (see also the definition of the rate coefficient in plasma as it is discussed in [39]). It is presumably not accidental that the density 10^{12} cm^{-3} is the same as the density at which the measured effective H_3^+ recombination rate coefficient changes its character. We have in mind that at temperatures below 300 K k_{sc} and α_{eff} are dependent on rotational excitation (ortho and para states) of H_2 and H_3^+ than also the condition for thermal equilibrium is more complex. We will come to this point again later.

Because a recombining plasma contains neutral molecules and atoms, collisions between ions and electrons are perturbed by the neutral particles, which can influence the observed effective plasma recombination rate. The perturbation could be significant if in an electron-ion collision a long-lived highly excited intermediate neutral molecule is formed (see the discussion in Refs. [23, 28]). If the third particle is an atom from the buffer gas, the probability of such a collision is proportional to its pressure and, as a consequence, the apparent recombination rate coefficient will be pressure dependent. Similar phenomena are well known from studies of ion-molecule association reactions, which can have a binary (e.g. radiative association) and/or three-body character depending on the lifetime of the complex. The rate of these processes can depend on pressure and temperature (e.g. associative reactions, see the discussion in [40]). Third-body perturbation of H_3^+ binary recombination in a plasma was already mentioned in our recent study [23]. In the present study, we show further experimental evidence for the phenomenon and further aspects of the theoretical interpretation, in conjunction with numerical calculation.

The rest of the article is organized as follows. First, we briefly describe the experiments in section II. Then we present new experimental results in section III, where we interpret the observed dependencies of the apparent binary recombination rate coefficients (α_{eff}) on hydrogen and helium pressure, and from that analysis, derive the

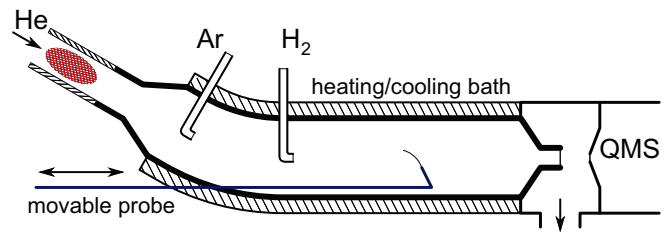


FIG. 1: Cryo-FALP. Plasma created in a microwave discharge is carried along the flow tube by helium carrier/buffer gas (from left to right in the drawing). After addition of Ar (via the indicated gas inlet) the plasma is converted from He_2^+ dominated to Ar^+ dominated. Further downstream H_2 is injected to an already-relaxed plasma (with thermalized electrons) and an H_3^+ dominated plasma is formed. The electron density decay downstream from the hydrogen entry port is monitored by an axially movable Langmuir probe.

binary and ternary recombination rate coefficients. Finally, in section IV we introduce our theoretical description of ternary recombination of an H_3^+ plasma, present our calculation of the lifetimes of the long-lived neutral molecules H_3^* formed in the electron-ion collisions, and estimate the rate coefficient for the ternary channel of H_3^+ recombination. Section V summarizes our conclusions.

II. EXPERIMENTS

For measurements of pressure and temperature dependences of the H_3^+ recombination rate we have built the Cryo-FALP apparatus, designed to operate in the range 77–300 K and at helium pressures adjustable from ~ 400 to ~ 2000 Pa. UHV technology and high buffer gas purity (the level of impurities is < 0.1 ppm) are used in the Cryo-FALP (Fig. 1).

The Cryo-FALP apparatus is a low temperature high pressure variant of the standard FALP apparatus [41]. Here we will just describe the essential features of the new construction. In Cryo-FALP, plasma is created in a microwave discharge (10–30 W) in the upstream glass section of the flow tube (at 300 K). Because of the high pressure, He^+ ions formed by electron impact then react in a three-body association reaction with two atoms of helium, and a He_2^+ dominated plasma is formed. Downstream from the discharge region, Ar is added to He_2^+ dominated afterglow plasma to remove helium metastable atoms (He^m in Fig. 2) formed in the discharge and to form Ar^+ dominated plasma (see details in [3, 4, 12, 13]). Via the second entry port situated approximately 35 ms downstream from the Ar entry port, hydrogen (diluted in He) is introduced into the plasma, which at this point is already cold. Note that the position in the flow tube is linked to the decay time. In a sequence of ion-molecule reactions, an H_3^+ dominated plasma is formed shortly after the second entry port.

We have used a numerical model to simulate the process of formation of H_3^+ dominated plasma. Examples

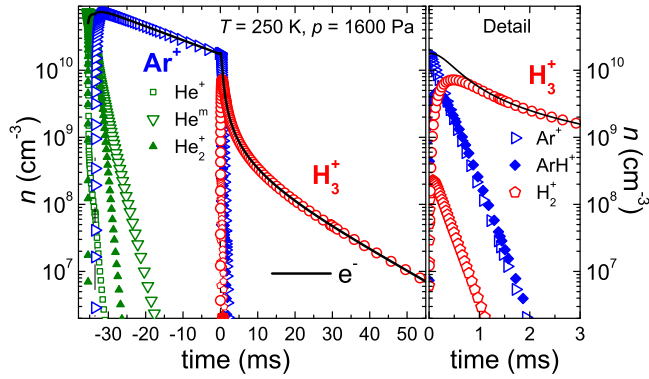


FIG. 2: Left panel: Calculated dependences of ion formation and plasma decay in FALP after addition of Ar ($7.7 \times 10^{12} \text{ cm}^{-3}$) and H₂ ($5 \times 10^{12} \text{ cm}^{-3}$). Argon was added in the flow tube 33 ms before H₂. The time scale origin is set at the position of the hydrogen injection port. The right panel focuses on a narrow time interval corresponding to a transition from Ar⁺ dominated to H₃⁺ dominated plasma after adding hydrogen.

of ion density evolutions calculated within the model for conditions typical for the present Cryo-FALP experiments are shown in Fig. 2. Similar calculations were carried out for all of our experiments presented in this work. Argon also plays a role in plasma relaxation and in formation of H₃⁺ ions. However, when an H₃⁺ dominated plasma has already been formed, Ar does not play any role (in contrast with He) because its density is at least four orders of magnitude lower than the helium density. Downstream from the Ar entry port the flow tube is thermally insulated and cooled to the desired temperature by liquid nitrogen. Because theory suggests a very strong temperature dependence of the process of interest, we monitored carefully the temperature of the flow tube. An axially movable Langmuir probe [42] is used to measure the electron density decay downstream from the hydrogen entry port [24]. Electron energy distribution functions (EEDF) were checked along the flow tube to characterize plasma relaxation during the afterglow time [34, 43]. Recombination of O₂⁺ (“benchmark ion” [3, 4]) was used for calibration of the Langmuir probe over a broad range of pressures.

An advanced analysis was used to fit the decay curves [3, 17, 44] with the purpose to obtain recombination rate coefficients from the measured decay of electron densities. In the analysis we have assumed that once an H₃⁺ dominated plasma is formed, the plasma decay can be described by a single value of the recombination rate coefficient, which we call the effective apparent binary recombination rate coefficient, α_{eff} . The plasma decay can then be described by the balance equation with a recombination and a diffusion loss terms:

$$\frac{dn_e}{dt} = -\alpha_{\text{eff}} n_e n_+ - \frac{n_e}{\tau_D} = -\alpha_{\text{eff}} n_e^2 - \frac{n_e}{\tau_D}, \quad (1)$$

where n_e and n_+ are electron and ion densities, respec-

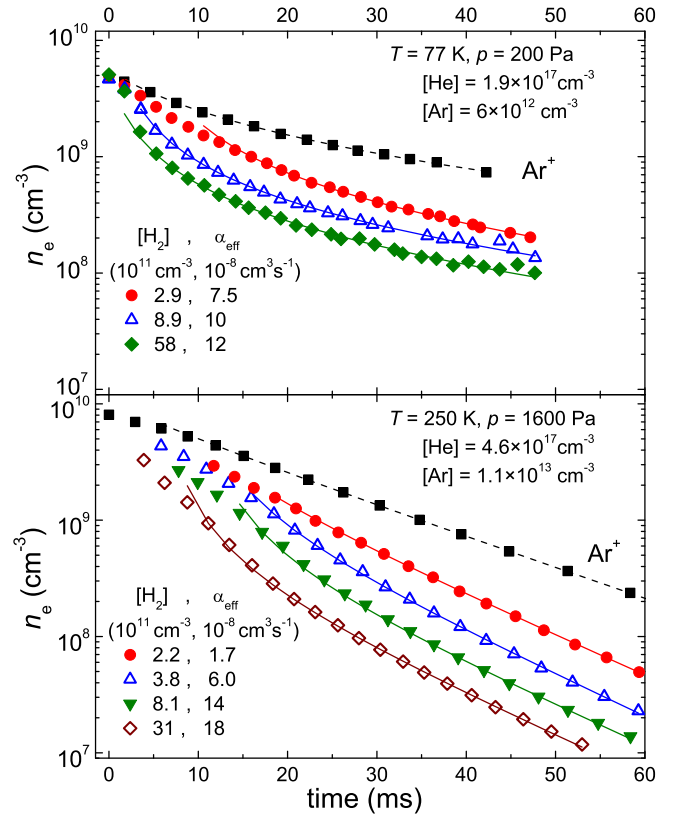


FIG. 3: Examples of electron density decay curves measured in the H₃⁺ dominated plasma at several hydrogen densities. Upper panel: Cryo-FALP experiment. Lower panel: FALP experiment. The effective recombination rate coefficients obtained at different hydrogen densities are indicated. For comparison, both panels also show the decay curves (rectangles) obtained in the Ar⁺ dominated plasma with [H₂] = 0.

tively. We assume that plasma is quasineutral ($n_e = n_+$). The constant τ_D characterizes the ambipolar diffusion during the afterglow. The recombination of H₃⁺ ions at temperatures below 300 K depends strongly on the rotational excitation of ions. The assumption about the constant value of α_{eff} must be discussed for particular experimental conditions.

In the present experiments we use helium densities in the range [He] $\sim 6 \times 10^{16} - 6 \times 10^{17} \text{ cm}^{-3}$ and hydrogen densities in the range [H₂] $\sim 10^{11} - 10^{14} \text{ cm}^{-3}$. In the Cryo-FALP and other experiments discussed we use normal hydrogen (n-H₂) i.e. the mixture of ortho and para-H₂ corresponding to 300 K (approximately 25% of para H₂). The variation of the ortho/para-H₂ ratio with temperature in the interval 77 K–300 K is not significant for the results of the present experiments. (In thermal equilibrium at 100 K the fraction of para H₂ is $\sim 38\%$, and at 77 K the fraction is $\sim 50\%$).

III. EXPERIMENTAL RESULTS

We monitored decay of the afterglow plasma in a He/Ar/H₂ mixture at different temperatures and over a broad range of helium and hydrogen densities. Examples of decay curves measured at 77 K and at 250 K at several hydrogen densities are plotted in Fig. 3. The dependence of the decay rate on hydrogen density is evident. The obtained apparent recombination rate coefficients (α_{eff}) depend on all three parameters $\alpha_{\text{eff}}(T, [\text{H}_2], [\text{He}])$. It clearly indicates that the observed “deionization process” is not pure binary dissociative recombination. In Fig. 3 we have also plotted the decay curves measured in a He/Ar afterglow plasma dominated by Ar⁺ ions at 77 K and at 250 K in otherwise very similar conditions. At 250 K (see lower panel) the decay curve is exponential (straight line in the semilogarithmic plot) because recombination of these atomic ions is very slow and the decay is governed by ambipolar diffusion. At 77 K (see upper panel of Fig. 3) we observe a faster decay during the early afterglow (at higher electron densities). We assume that this faster decay is primarily due to collisional radiative recombination (CRR) [45, 46] and partly also due to the formation of Ar₂⁺ ions (in three-body association at low temperatures) followed by immediate recombination of these ions [47]. The rate of the decay is comparable with the rate calculated for the CRR at ~ 85 K.

The apparent binary recombination rate coefficients (α_{eff}) obtained from measured decay curves in the H₃⁺ dominated plasma are plotted as functions of hydrogen density in Fig. 4. Examples of the data obtained in other experiments (FALP, AISA and TDT-CRDS) are also included in Fig. 4. Below we summarize the data plotted in Fig. 4.

Upper panel:

1. 77 K, Cryo-FALP. At a fixed flow tube temperature ($T = 77$ K) and at fixed $[\text{He}] = 1.9 \times 10^{17} \text{ cm}^{-3}$, the dependence of α_{eff} on H₂ density was measured from $[\text{H}_2] \sim 2 \times 10^{11} \text{ cm}^{-3}$ to $\sim 10^{13} \text{ cm}^{-3}$. Then, for several other helium densities the recombination rate coefficient was only measured in a limited range of hydrogen densities close to $[\text{H}_2] \sim 10^{13} \text{ cm}^{-3}$. We plot only a few examples.
2. 100 K, TDT-CRDS. The H₃⁺ ion density was measured by using laser absorption spectroscopy (CRDS technique). During the discharge pulse and during the recombination dominated afterglow, the ion temperature was determined from the Doppler broadening of an absorption line. The details of such experiments can be found in [48].
3. 330 K, TDT-CRDS. The absorption spectroscopy technique (CRDS) was used to measure the temperature and density of the recombining H₃⁺ ions [25, 26, 48]. Relatively high hydrogen density was used in these experiments. Therefore, an extrapolation had to be carried out in order to obtain

α_{eff} for lower hydrogen densities (see the discussion below). For details of this extrapolation see the discussion in [24, 47]. In some experiments, the He temperature was determined by measuring the Doppler broadening of the H₂O line [48]. We have also assumed that the temperatures of H₂O and He are identical. The H₂O density is very low but sensitivity of CRDS is very high for this molecule.

Lower panel:

4. 130 and 230 K, AISA. Examples of data measured with AISA. The data were measured at a fixed temperature and at a fixed pressure as a function of hydrogen density.
5. 170, 195, 250 K, FALP. Three different versions of FALP designed to work at high He pressures were used in these experiments.
6. 300 K, Experiment by Laube *et al.* [49]. Low pressure FALP experiment: $[\text{H}_2] = 2 \times 10^{14} \text{ cm}^{-3}$, $[\text{He}] = 1.6 \times 10^{16} \text{ cm}^{-3}$, obtained α_{eff} is $7.8 \times 10^{-8} \text{ cm}^3 \text{ s}^{-1}$.
7. 295 K, experiment by Gougousi *et al.* [15]. In this FALP experiment the dependence of the recombination rate coefficient on $[\text{H}_2]$ was observed. The helium pressure was about 130 Pa.
8. 300 K, theory [8, 38]. The value calculated for binary dissociative recombination (for $[\text{H}_2] = 0$).

Notice that in certain experiments the rate coefficients were measured over a limited range of hydrogen densities. In our experiments, we have covered the $10^{10} \text{ cm}^{-3} < [\text{H}_2] < 10^{16} \text{ cm}^{-3}$ range (AISA, FALP, Cryo-FALP, TDT-CRDS).

In the measured dependences shown in Fig. 4 we distinguish three clearly different regions of hydrogen densities that exhibit specific behavior of α_{eff} as a function of $[\text{H}_2]$. We indicate these regions as $N < 1$, $N > 1$, and $N \gg 1$. The “vertical shifts” for some dependences in Fig. 4 (such as the data presented with open and full triangles in the lower panel) are discussed below. We characterize the three regions as follows.

1. $[\text{H}_2] < 10^{12} \text{ cm}^{-3}$, $N < 1$. At these hydrogen densities α_{eff} decreases with decreasing hydrogen density. At such conditions the H₃⁺ ions formed by an exothermic proton transfer (from ArH⁺ or H₂⁺ to H₂) do not have enough collisions with H₂ to establish ortho/para-H₃⁺ thermal equilibrium prior to their recombination (see e.g. the discussion in [36, 37, 38]). The number of these H₂ + H₃⁺ collisions that a H₃⁺ ion will undergo prior to its recombination with an electron (at typical conditions of the discussed afterglow experiments) is indicated in the Fig. 4 by number N . If $N < 1$, the decay of the plasma caused by the recombination (at a given electron density) is faster than the

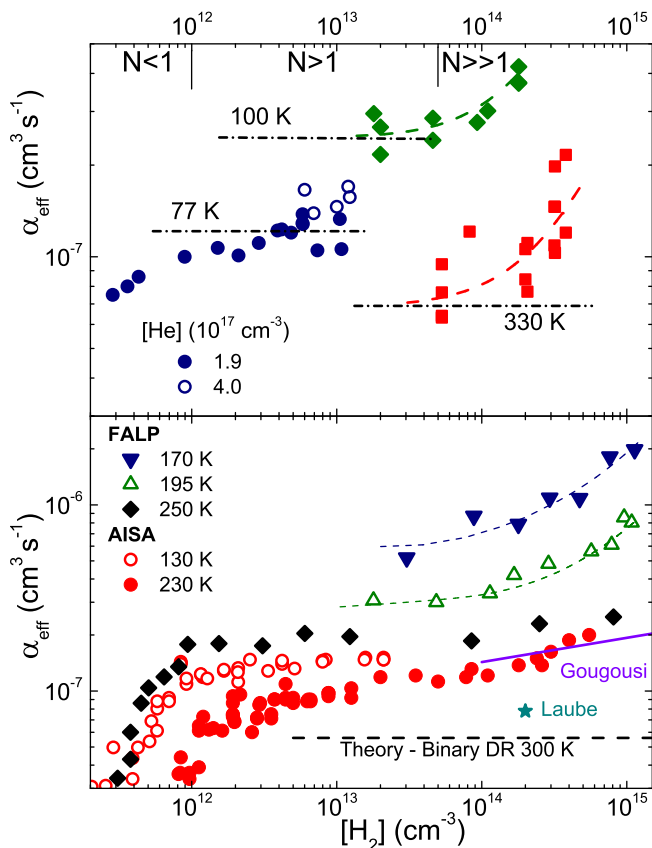


FIG. 4: Measured dependencies of the effective recombination rate coefficient of H_3^+ ions on hydrogen density. The data obtained by Cryo-FALP and TDT-CRDS are plotted in the upper panel. The data obtained in other experiments are plotted in the lower panel. We have also plotted examples of data obtained in our previous studies using: AISA, TDT-CRDS and FALP. The FALP data by Laube *et al.* [49] and Gougousi *et al.* [15] are plotted for comparison. Additionally, we show the value of the theoretical recombination rate coefficient calculated for binary dissociative recombination (DR), $\alpha_{\text{Bin}}(300 \text{ K})$ [8, 38]. Note that for this theoretical result, only the binary DR process is considered, and as such it cannot depend on the hydrogen density.

rate of rethermalization. Therefore, in this non-equilibrium regime, the individual state composition of H_3^+ afterglow plasma is different along the flow tube because the effective recombination rate depends on the absolute value of electron density, which varies along the length of the tube. By “state composition” we mean not only the kinetic energy distribution, which is established in collisions with He atoms with a nearly collisional rate, but also the rotational and ortho- H_3^+ /para- H_3^+ state distribution. A quantitative description of this particular regime would require a much deeper theoretical analysis.

- $10^{12} \text{ cm}^{-3} < [\text{H}_2] < 5 \times 10^{13} \text{ cm}^{-3}$, $N > 1$. In this regime, the measured rate coefficients are

nearly independent of $[\text{H}_2]$. On the basis of the same arguments mentioned above, it is clear that at $[\text{H}_2] > 10^{12} \text{ cm}^{-3}$, the H_3^+ ion (formed shortly after hydrogen is injected) has several collisions with H_2 prior to its recombination with an electron. Because only some collisions lead to a change in rotational excitation of H_3^+ or in ortho \leftrightarrow para transitions [36, 37]), we assume that if $[\text{H}_2] > 10^{12} \text{ cm}^{-3}$ the recombining ions in the flow tube will be in thermal equilibrium corresponding to the hydrogen temperature, which is assumed to be equal to the helium temperature. Because of the independence of α_{eff} on $[\text{H}_2]$ we will call this region the “saturated region”. The boundaries of the saturated region depend on actual helium pressure, temperature and electron density. The region is broad enough to find conditions where the value of α_{eff} is nearly constant (the plateau part of the $\alpha_{\text{eff}}([\text{H}_2])$ dependence). Depending on experimental conditions we have covered either the whole saturated region or in some cases just a part of it.

- $[\text{H}_2] > 5 \times 10^{13} \text{ cm}^{-3}$, $N \gg 1$. Here the measured recombination rate coefficient increases with hydrogen pressure. This behavior is caused by a formation of H_5^+ ions and their fast recombination. The process is temperature and pressure dependent (see details in [24, 50, 51, 52]). Because of the strong temperature and pressure dependence of ternary association, the onset of this region depends on these parameters.

At first sight the “vertical shifts” of the dependences plotted in Fig. 4 are very chaotic. We demonstrate below that they arise because the apparent binary recombination rate coefficient (α_{eff}) depends not only on hydrogen density and temperature but also on the helium density. In addition, we also show that the temperature dependence of α_{eff} is not monotonic.

We will not discuss the $N < 1$ region here. However, in connection with the data obtained at 77 K we want to point out one difference from the data obtained at higher temperatures. In all high temperature experiments made at $[\text{H}_2] < 10^{12} \text{ cm}^{-3}$, we have observed a fast decrease of α_{eff} with decreasing $[\text{H}_2]$ (see e.g. the FALP data measured at 250 K in the lower panel of Fig. 4). In measurements at 77 K using Cryo-FALP (see the upper panel of Fig. 4) the decrease is substantially smaller. The difference can be partly associated with the effect of collisional radiative recombination (CRR) at 77 K. At $[\text{H}_2] \sim 10^{13} \text{ cm}^{-3}$ when the overall recombination rate coefficient $\alpha_{\text{eff}}(77 \text{ K}) > 1.0 \times 10^{-7} \text{ cm}^3 \text{ s}^{-1}$ we can neglect the influence of these processes (see the upper panels of Fig. 3 and Fig. 4).

Figure 4 has a great deal of information, because it actually shows α_{eff} as a function of three variables T , $[\text{H}_2]$, and $[\text{He}]$. By analyzing the data we found the form of the function $\alpha_{\text{eff}}(T, [\text{H}_2], [\text{He}])$ in the “saturated region”, i.e. for the plasma where the H_3^+ ions before recombining

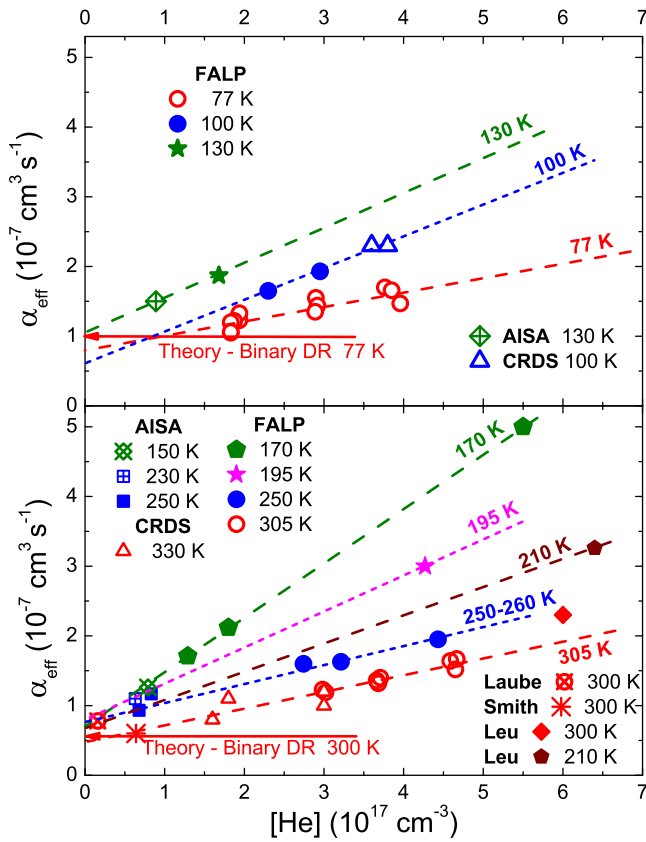


FIG. 5: The effective binary recombination rate coefficients (α_{eff}) measured at the stated temperatures are shown as functions of the helium density. Upper panel: Low temperature data – Cryo-FALP (77 K), TDT-CRDS & Cryo-FALP (100 K) and AISA & FALP (130 K). The horizontal line indicates the theoretical value for binary dissociative recombination at 77 K [8, 38]. For details, see the summary in the text. Lower panel: Higher temperature data – Cryo-FALP (305 K), FALP (250–260 K, 170 and 195 K), TDT-CRDS (330 K), AISA (250–260, 230 and 150 K). Individual points measured in other laboratories: Smith and Spänzel [16], Laube *et al.* [49], Leu *et al.* [51] (see description in the text). The horizontal line indicates the theoretical value for the binary dissociative recombination of H_3^+ at 300 K [8, 38].

undergo a sufficient number of “state changing collisions” with H_2 to reach thermal equilibrium. For a better analysis of the experimental data we plotted α_{eff} measured at a fixed temperature as a function of helium density. The rate coefficients measured in the three principally different afterglow experiments at several different temperatures at hydrogen densities corresponding to the saturated region are plotted as functions of helium density in Fig. 5.

We briefly summarize the data plotted in Fig. 5. Upper panel:

1. 77 K, Cryo-FALP. The data from measurements at $[\text{H}_2] \sim 10^{13} \text{ cm}^{-3}$ at different $[\text{He}]$ (see upper panel of Fig. 4). The experiment was intended as a mea-

surement of the pressure dependence at a fixed temperature. The straight line is the best fit through the measured data.

2. 100 K, TDT-CRDS. The values plotted were obtained from the measured dependences of α_{eff} on hydrogen density as limits approaching the saturated region (see upper panel of Fig. 4). More details are given in [53].
3. 100 K, Cryo-FALP. The present measurements.
4. 130 K, AISA. The data were obtained from the measured dependence of α_{eff} on hydrogen density (see lower panel of Fig. 4). More details is given in [48].
5. 130 K, Cryo-FALP. The present measurements.
6. 77 K Theory. The horizontal line indicates the theoretical value of the recombination rate coefficient for binary dissociative recombination (DR) of H_3^+ at 77 K [8, 38].

Lower panel of Fig. 5:

7. 150, 230 and 250 K, AISA. The values shown were obtained from measured dependencies of α_{eff} on hydrogen density as limits approaching the saturated region (see upper panel of Fig. 4 and Ref. [48]). The accuracy of the values is high because the values were obtained from a number of measurements.
8. 170 and 195 K, FALP & AISA. The FALP data were obtained similarly to the AISA data, i.e. as limits approaching the saturated region. The straight lines connect the measured FALP points with the AISA points, which are obtained by an extrapolation of the data measured by AISA at 130–230 K.
9. 250–260 K, AISA & FALP. Compilation of data from several experiments (for details see Refs. [23, 54]).
10. 305 K, Cryo-FALP. The data were obtained by directly changing the helium pressure in the flow tube.
11. 330 K, TDT-CRDS. The values were obtained as limits approaching the saturated region (see upper panel of Fig. 4).
12. 210 and 300 K, Leu *et al.* [51]. In the experiment a microwave technique was used to measure the electron density. The values $2.3 \times 10^{-7} \text{ cm}^3 \text{ s}^{-1}$ and $3.3 \times 10^{-7} \text{ cm}^3 \text{ s}^{-1}$ for 300 K and 210 K respectively (pressure $\sim 2.6 \text{ kPa}$) were taken from Figs. 2 and 4 of Ref. [51].
13. 300 K, Laube *et al.* [49], a FALP (FALP-MS) experiment. The measured value is $\alpha_{\text{eff}} = 7.8 \times$

$10^{-8} \text{ cm}^3\text{s}^{-1}$ (see Fig. 4). He pressure was $\sim 70 \text{ Pa}$. Used hydrogen density corresponds to the saturated region.

14. 300 K, Smith & Spanel [16] a FALP experiment. We show the value from their plot of the recombination rate coefficient as a function of position along the flow tube (in Fig. 4). In the conditions that arise shortly after injection of hydrogen, Smith & Spanel measured the value $\alpha_{\text{eff}} \sim 6 \times 10^{-8} \text{ cm}^3\text{s}^{-1}$ for a relatively long time (see Fig. 4 in [16]). Further downstream, they obtained a lower value of the recombination rate coefficient. The helium pressure was $\sim 260 \text{ Pa}$.
15. 300 K, Gougousi *et al.* [15]. We did not include their value in the graph because their measurements were at hydrogen densities too high and therefore out of the saturated region. We only mention their experiment in order to show that we included this study in our considerations.

With regard to data obtained by Laube *et al.* [49], Smith & Spanel [16], and Gougousi *et al.* [15], we have not analyzed their experiments in full detail. However, it is clear from their studies that, in agreement with our experimental data, there is a general trend: The effective rate constant α_{eff} increases with the increase of helium density (in the temperature interval covered). In Refs. [15, 16, 49] the authors used relatively low helium pressures. Therefore, the increase of α_{eff} with $[\text{He}]$ was not as large as we observe in our measurements, such as Cryo-FALP. Very high pressure was used in [51]. As a result, they obtained large α_{eff} in agreement with the trend.

The experimental data plotted in Fig. 5 show that the apparent effective binary recombination rate coefficient α_{eff} measured at a fixed temperature depends linearly on helium density. We will discuss a possible recombination mechanism below, but at this point we can assume that the process has a binary character at very low $[\text{He}]$, whereas with increasing $[\text{He}]$ the helium assisted ternary process begins to contribute substantially to the overall recombination deionization process. Therefore, we can write for the observed linear dependence

$$\alpha_{\text{eff}} = \alpha_{\text{Bin}}(T) + K_{\text{He}}(T)[\text{He}] \quad (2)$$

in terms of the rate coefficient $\alpha_{\text{Bin}}(T)$ for binary recombination and the rate coefficient $K_{\text{He}}(T)$ for ternary He-assisted recombination. The two coefficients depend on temperature. Note that for some temperatures we have the FALP data (e.g. 77 K), for others we used AISA & FALP data, and also the TDT-CRDS data. The AISA data were obtained at low helium densities. The FALP data were taken at high helium densities and in most cases we could vary the He pressure in the FALP experiments. We extrapolate the data from AISA to temperatures 170 K and 195 K. Then we plot a straight line through these new points (obtained by the extrapolation) and the corresponding points measured by FALP

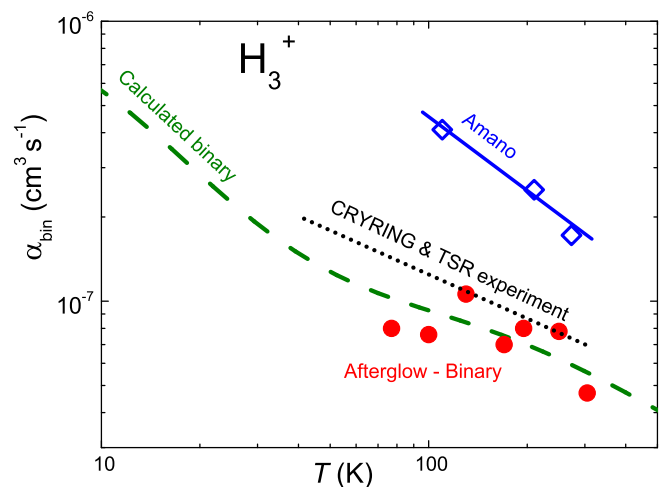


FIG. 6: The H_3^+ binary recombination rate coefficient measured in the present study (circles). The theoretical values shown (the dashed line) are calculated for relative populations of para and ortho H_3^+ corresponding to the thermal distribution at the stated T [8, 38]. The dotted line indicates values calculated from cross sections obtained in storage ring experiments [10, 11, 55] using cold ion sources. The present values are obtained as limits approaching the saturated region at low helium density from plots in Fig. 5. We also show the data (squares) obtained by Amano in pure hydrogen [14]. Further details are given in the text.

(see lower panel in Fig. 5). Using the straight line fits we obtain experimental values for α_{Bin} and K_{He} at 170 K and 195 K.

The obtained values of the binary recombination rate coefficients $\alpha_{\text{Bin}}(T)$ are plotted in Fig. 6 as a function of temperature. We also show on Fig. 6 thermal rate coefficients calculated for binary dissociative recombination of H_3^+ [8, 38]. The agreement is very good. Note that the data for 170 K and 195 K (at high $[\text{He}]$) were published [24, 48] before the calculation [8]. The data for 250 K was partially obtained [3] also before the calculations. The pressure dependence of the 250 K data set was measured after [23] the calculations were published. Some data for 100 K and 300 K were also measured earlier, using CRDS [25, 53].

Figure 6 also presents the data obtained by Amano using absorption spectroscopy [14] in experiments made with pure hydrogen at $\sim 40 \text{ Pa}$ ($[\text{H}_2] \sim 10^{16} \text{ cm}^{-3}$) used as a buffer gas. The large values of the measured recombination rate coefficients indicate that the molecular hydrogen is a more effective three body partner (with an effective ternary rate constant of order of $10^{-23} \text{ cm}^6\text{s}^{-1}$) than helium, which is not surprising because H_2 has rotational and vibrational degrees of freedom.

We have also checked that the observed linear pressure dependence of α_{eff} is not associated with the Langmuir probe operating at different pressures from 40 to 2600 Pa. For this test we have used the same probe to measure the recombination rate coefficient for O_2^+ ions

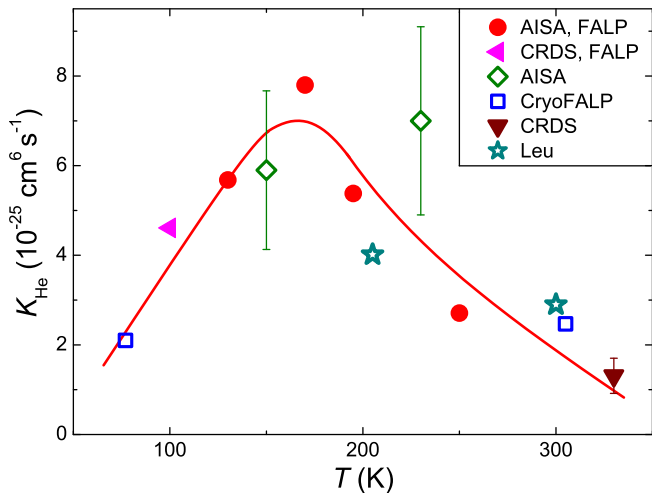


FIG. 7: The measured ternary recombination rate coefficient, $K_{\text{He}}(T)$, for helium assisted recombination of H_3^+ with electrons. The legend indicates the experiments used to extract the data. The plotted line is shown merely to guide the eye.

[3, 4]. Our assumption was that $\alpha_{\text{O}_2^+}$ is pressure independent because O_2^+ recombination is a direct binary (electron–ion) process. We have also studied the pressure dependence of recombination rate coefficients for HCO^+ and DCO^+ ions [54] using the probe. For both cases (O_2^+ and $\text{HCO}^+/\text{DCO}^+$) we observed no pressure dependence. Our HCO^+ and DCO^+ rate coefficients are in good agreement with results of Leu *et al.* [51] and Amano [14] measured by different techniques. Leu *et al.* [51] used a microwave technique to determine electron densities but obtained results are consistent with our observation.

The ternary rate coefficients obtained from the data plotted in the Fig. 5 are presented in Fig. 7 as a function of buffer gas temperature. The values obtained for 300 K are: $\alpha_{\text{Bin}}(300 \text{ K}) = (4.7 \pm 1.5) \times 10^{-8} \text{ cm}^3 \text{ s}^{-1}$, $K_{\text{He}}(300 \text{ K}) = (2.5 \pm 1.2) \times 10^{-25} \text{ cm}^6 \text{ s}^{-1}$. The figure shows that the ternary rate coefficient has a maximum at $\sim 170 \text{ K}$. Towards lower temperatures the rate coefficient is decreasing. This is a surprising result if one takes into account studies of ternary association processes. For such processes the ternary rate coefficients decrease monotonically with temperature (see Refs. [56, 57, 58]).

We briefly summarize the data plotted in Figure 7:

1. 77 K, Cryo-FALP. The data obtained from the pressure dependence measured in the present experiments at 77 K. See upper panels of Figs 3, 4, and 5. The value of K_{He} was obtained from measurements that were repeated many times.
2. 100 K, Cryo-FALP & TDT-CRDS. The data obtained by a combination of the values measured in two experiments. The TDT-CRDS values are based on measurements of the ion density evolution during the afterglow using CRDS absorption

spectroscopy. (see the upper panels of Figs. 4 and 5). In order to calculate the ion density from the absorption signal, thermodynamic equilibrium was assumed. The assumption should be valid at the hydrogen densities used. The Cryo-FALP values were measured in the present experiments (upper panel of Fig. 5).

3. 130, 170, and 195 K, AISA & FALP. Data obtained in two experiments (Fig. 5).
4. 150 and 230 K, AISA. AISA was used to measure the dependence of α_{eff} on hydrogen density over a broad range including the “saturated region”, (lower panel of Fig. 4). From these measurements, average values of the recombination rate coefficient in the “saturated region” have been obtained for several temperatures (see Fig. 5). These data are very accurate because the measurements have been done many times at a fixed temperature. As we did not measure the dependence on helium pressure in the AISA experiments, we calculated K_{He} using Eq. (2) with the current theoretical value for $\alpha_{\text{Bin}}(T)$. The data have been obtained at low pressures, 160–330 Pa. Therefore, the ternary rate coefficients extracted from this data have large error bars.
5. 250–260 K, FALP & AISA. These data were obtained in several experiments. A detailed description was given in our previous publication [23] but there is one key difference: In that study, [23] the “260 K” plot also included values obtained at temperatures close to but different from 260 K; the data shown there for $\alpha_{\text{eff}}(260 \text{ K})$ were recalculated from the measured values, assuming a $T^{-0.5}$ dependence, which is a small correction. Because of the additional experiments with Cryo-FALP the recalculation procedure was not necessary in the present work. Now it is clear that α_{eff} depends on both temperature and pressure; in the vicinity of 260 K the temperature dependence is steeper than $T^{-0.5}$.
6. 305 K, Cryo-FALP. In this experiment the pressure dependence was measured (see Fig. 5).
7. 330 K, TDT-CRDS. The measurements were similar to those at 100 K (upper panel of Fig. 4 and lower panel of Fig. 5). Two different absorption lines were used in these studies. We have obtained the same value of the rate coefficient α_{eff} using either absorption line.
8. 210 and 300 K, Data from Leu *et al.* [51]. (see Fig. 5). We have utilized the current theoretical binary recombination rate coefficients for 210 and 300 K and Eq. 2 to obtain the corresponding ternary rate coefficients.

IV. THEORETICAL MODEL FOR HELIUM-ASSISTED NEUTRALIZATION OF THE AFTERGLOW PLASMA

It is possible to estimate theoretically the rate coefficient, Eq. (2), of the He-assisted recombination of H_3^+ with electrons in the following way. To stress that it is an estimated value, we use symbol K^{3d} for the theoretical coefficient.

He-assisted recombination is treated as a two step process. In electron- H_3^+ scattering, rotational autoionization resonances of the neutral molecule H_3^* play an important role (see, for example Ref. [7, 59]). The star next to H_3 refers to the unstable character of these autoionizing resonances. Such resonances with angular momentum $l = 1$ could be very quite broad due to the high probability to capture an electron into the $l = 1$ partial wave, but they normally contribute relatively little to the two-body, $\text{H}_3^+ + e^-$ recombination [7], because almost always, such resonances decay back into a free electron and an H_3^+ ion. As we demonstrate below, lifetimes of some of these resonances can be quite long. If, during their lifetime, the H_3^* molecule collides with a helium atom, the collision can lead to a change in the electronic state of the outer electron or in the rotational state of the H_3^+ ion and therefore, can make the autoionization process impossible (or, at least, much less probable than the dissociation of H_3). The overall rate coefficient for such He-assisted recombination is given by the formula derived in Ref. [23]:

$$K^{3d} = k_l \Delta t \alpha_* , \quad (3)$$

where α_* is the rate coefficient for the formation of H_3^* ; k_l is the rate coefficient for l -changing collisions between He and H_3^* leading to the eventual dissociation of H_3^* . Finally, Δt is the delay time in the $\text{H}_3^+ + e^-$ collision in the sense introduced by Smith [60]: it is an additional time that the electron spends near the ion in the modified Coulomb potential compared to the collisional time in a pure Coulomb potential. The delay time and the coefficient α_* are substantially different from zero only near resonances. Therefore, the three-body rate coefficient discussed above is expected to vary resonantly as a function of collisional energy.

We stress here that the rate constants k_l , and α_* described above depend on the corresponding scattering energies (and defined as usual as cross-sections multiplied by relative velocities). They are not yet thermally averaged over the Maxwell-Boltzmann distribution. Correspondingly, the ternary rate constant K^{3d} in Eq. (3) depends on two energies: the energy E of the $\text{H}_3^+ + e^-$ collision due to the dependence of Δt and α_* on E ; and the energy E_{He} of collision between He and H_3^* due to the dependence of k_l on E_{He} . In this approach, however, the coefficient $k_l(E_{\text{He}})$ is considered to be constant over the energy interval of interest. The rate coefficient α_* in our estimation is evaluated as $v\sigma(E)$, where $v = (2E/m)^{1/2}$ is the relative velocity, $\sigma(E)$ is the cross-section for the

process leading to the delay time, m is the reduced mass of the $\text{H}_3^+ + e^-$ system.

For the following discussion, we assume that at a given energy E , there could be several open $\text{H}_3^+ + e^-$ ionization channels ($i = 1, 2 \dots n_o$). Such a situation is possible for the conditions of the present experiment. If there are several open channels, the three-body coefficient K^{3d} above should be averaged over the incident channels and summed over the final ones. If the incident ionization channel (before collision) is denoted by the index i , and the final one (following the collision) is j , then the corresponding rate coefficient for the three-body recombination during the $i \rightarrow j$ inelastic collision is given by

$$k_l \Delta t_{ji} \sqrt{2E/m} \sigma_{ji}(E) , \quad (4)$$

with $\sigma_{ji}(E)$ being the cross-section for the inelastic collision. The delay time Δt_{ji} for the process is an element of the delay-time matrix $\Delta \mathbf{t}$ as it is introduced and discussed by Smith [60]:

$$\Delta t_{ji} = \Re \left[-i\hbar \frac{1}{S_{ji}} \frac{dS_{ji}}{dE} \right] , \quad (5)$$

where S_{ji} is an element of the scattering matrix for the $i \rightarrow j$ process. Notice a difference in conventions in the present paper and Ref. [60]: Here, the first index in each matrix denotes the final channel. The second index denotes the incident channel. In Ref. [60], the convention adopted was the opposite, i.e., the first index \sim incident channel, second index \sim final one.

The cross-section $\sigma_{ji}(E)$ is given by

$$\sigma_{ji}(E) = \frac{\hbar^2 \pi}{2mE} |S_{ji}|^2 . \quad (6)$$

Using equations (4, 5, 6) and taking the sum over the final ionization channels j , we obtain the three-body rate coefficient K_i^{3d} if the initial state of the $\text{H}_3^+ + e^-$ system is i :

$$\begin{aligned} K_i^{3d} &= k_l \sum_{j=1}^{n_o} \Re \left[-i\hbar \frac{1}{S_{ji}} \frac{dS_{ji}}{dE} \right] \sqrt{2E/m} \frac{\hbar^2 \pi}{2mE} |S_{ji}|^2 \\ &= k_l (2E)^{-1/2} m^{-3/2} \hbar^2 \pi \sum_{j=1}^{n_o} \Re \left[-i\hbar \frac{1}{S_{ji}} \frac{dS_{ji}}{dE} \right] |S_{ji}|^2 \end{aligned}$$

The sum in the second line can be simplified as [60]

$$\begin{aligned} \sum_{j=1}^{n_o} \Re \left[-i\hbar \frac{1}{S_{ji}} \frac{dS_{ji}}{dE} \right] &= \sum_{j=1}^{n_o} \Re \left[-i\hbar S_{ji}^\dagger \frac{dS_{ji}}{dE} \right] \\ &= -i\hbar \left(S^+ \frac{dS}{dE} \right)_{ii} = Q_{ii} , \quad (7) \end{aligned}$$

where Q_{ii} is a diagonal element of the lifetime matrix introduced by Smith [60]

$$Q = -i\hbar S^\dagger \frac{dS}{dE} \quad (8)$$

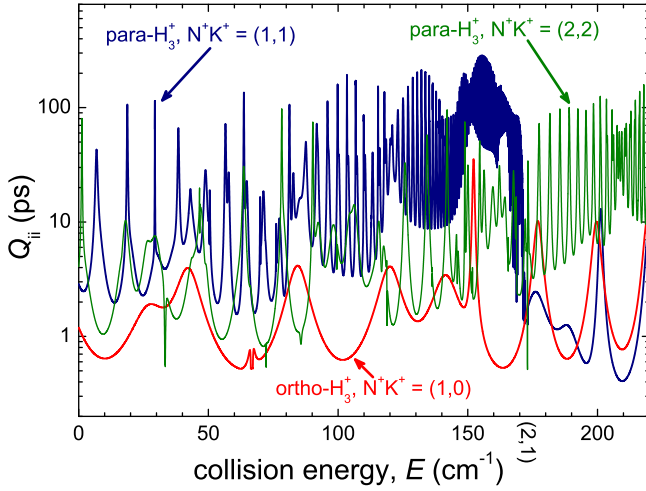


FIG. 8: Diagonal elements Q_{ii} of matrix Q for the three lowest (rotational) incident channels for the $e^- + \text{H}_3^+$ collisions. The rotational channels are $(N^+, K^+) = (11), (10),$ and (22) . Each maximum in Q_{ii} corresponds to an autoionization resonance. The lifetime of a resonances is given by $Q_{ii}/4$ evaluated at the maximum if there is only one channel open, $Q_{ii} = Q$.

and the product $S^\dagger \frac{dS}{dE}$ in the above equation is the regular matrix product. Due to the aforementioned difference in matrix index conventions, the order of the product is opposite to the one in Ref. [60]. Therefore, for K_i^{3d} we have

$$K_i^{3d} = k_l m^{-3/2} \hbar^2 \frac{\pi}{\sqrt{2E}} Q_{ii}, \quad (9)$$

or in atomic units

$$K_i^{3d} = k_l \frac{\pi}{\sqrt{2E}} Q_{ii}. \quad (10)$$

The next step in the evaluation of the three-body rate coefficient is the thermal average over incident ionization channels i and over the Maxwell-Boltzmann velocity distribution for a given temperature T . The average over incident channels is given by

$$\frac{\sum_i K_i^{3d} w_i \exp\left(-\frac{E_i}{k_B T}\right)}{\sum_i w_i \exp\left(-\frac{E_i}{k_B T}\right)}, \quad (11)$$

where $w_i = (2N_i^+ + 1)(2I_i + 1)$ is the statistical weight of the incident channel, N_i^+ and I_i are the angular momentum and the nuclear spin of the H_3^+ ion respectively, E_i is the energy of the incident channel (rotational energy of channel i). The average over the velocity (energy) distribution should be performed over the two energy variables, E and E_{He} , in $K_i^{3d}(E, E_{\text{He}})$. Because K_i^{3d} does not depend on E_{He} , the thermal averaging is reduced to the familiar two-body averaging integral over E only

$$\frac{2}{\sqrt{\pi}(k_B T)^3} \int_0^\infty K_i^{3d}(E) \exp\left(-\frac{E}{k_B T}\right) \sqrt{E} dE. \quad (12)$$

Combining the above equations, we obtain

$$\langle K_i^{3d} \rangle = \frac{2 \sum_i \int_0^\infty K_i^{3d} w_i \exp\left(-\frac{E+E_i}{k_B T}\right) \sqrt{E} dE}{\sqrt{\pi}(k_B T)^3 \sum_i w_i \exp\left(-\frac{E_i}{k_B T}\right)}, \quad (13)$$

or using the lifetime matrix element Q_{ii} ,

$$\langle K_i^{3d} \rangle = \sqrt{\frac{2\pi}{(k_B T)^3}} \frac{k_l \sum_i \int_0^\infty Q_{ii} w_i \exp\left(-\frac{E+E_i}{k_B T}\right) dE}{\sum_i w_i \exp\left(-\frac{E_i}{k_B T}\right)}. \quad (14)$$

The lifetime matrix Q is calculated using Eq. (8) from the scattering matrices obtained numerically [7, 8]. In practice, the scattering matrix $S^{(N)}$ (and matrix $Q^{(N)}$) are calculated for a fixed value of the total angular momentum N of the $\text{H}_3^+ + e^-$ system, which is the sum of the ionic N^+ and electronic l angular momenta. The contributions $Q_{ii}^{(N)}$ from different N should be accounted in Eq. (14), namely as

$$Q_{ii} = \frac{1}{2N^+ + 1} \sum_N (2N + 1) Q_{ii}^{(N)}. \quad (15)$$

The sum in the above equation runs over all N for which the incident channel i enters into the scattering matrix. Since the principal contribution to the rotational capturing of the electron comes from the $l = 1$ partial wave, the sum has three or less terms.

The collisional l -changing process is known to be relatively effective for excited atomic Rydberg states [61]. Because the $\text{H}_3^+(l = 1)$ molecules formed in the $\text{H}_3^+ + e^-$ collisions have a large principal quantum number ($n \sim 40$ – 100 , see Fig. 8), it is reasonable to use the atomic rates for l -changing collisions in our estimates. For $\text{Na}^* + \text{He}$ l -changing collisions [61] the experimental rate is $2.3 \times 10^{-8} \text{ cm}^3 \text{ s}^{-1}$. In our estimation, we use this value for k_l . Using the procedure described above and the value above for k_l we have calculated thermally averaged rate coefficient for the He-assisted recombination of H_3^+ . The coefficient is shown in Fig. 9 as a function of temperature. The overall agreement with the experimental rate coefficient shown in Fig. 7 is reasonable given the approximative approach that we used here. Below 150 K, the experimental curve drops down, but the theoretical (dashed) curve continues to grow. Interestingly, the curve for pure ortho- H_3^+ (dot-dashed curve) has a behavior similar to the experiment. In fact, it is possible that in the experiment the ortho and para- H_3^+ are not in thermal equilibrium at low temperatures. Our previous calculation [8] showed that the binary recombination rate of H_3^+ with electrons is much slower for ortho- H_3^+ than for para- H_3^+ : At low temperatures, due to fast recombination of para- H_3^+ the ratio ortho/para- H_3^+ could be larger than the one at thermal ortho/para equilibrium. In such a situation the averaged theoretical rate coefficient K^{3d} in Fig. 9 would be closer to the curve for ortho- H_3^+ , i.e. it would be lower at small T similar to the experimental behavior (Fig. 7).

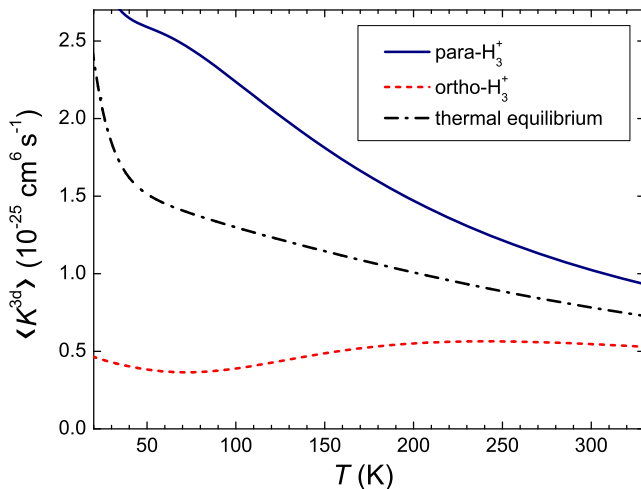


FIG. 9: Calculated thermally-averaged three-body rate coefficient $\langle K^{3d} \rangle$. The rate coefficients calculated separately for ortho and para- H_3^+ are very different. If the recombining plasma is not in thermal equilibrium with respect to ortho/para ratio, the averaged rate coefficient (dashed) could be very different from the one shown.

V. CONCLUSIONS AND DISCUSSION

We have studied recombination of H_3^+ ions in an afterglow plasma, in the presence of a helium buffer gas with a small admixture of molecular hydrogen. The helium densities were in the range $0.5 - 6 \times 10^{17} \text{ cm}^{-3}$ and hydrogen densities $1 - 100 \times 10^{12} \text{ cm}^{-3}$. In such conditions the H_3^+ ions formed in the plasma have several collisions with H_2 before they recombine with electrons. Thus, we assume that in these conditions the ions are in ortho/para thermal equilibrium. The apparent binary recombination rate coefficient α_{eff} was measured as function of hydrogen and helium densities for several temperatures in the 77–330 K range. From the experimental data we have derived the binary and ternary recombination rate coefficients and their dependences on temperature. The measured binary recombination rate coefficient is in good agreement with recent theoretical calculation over the whole covered temperature range (77–330 K). Therefore, for the first time, the recombination rate coefficients obtained in afterglow plasma experiments agree with storage ring experiments and with theoretical values. As we have demonstrated in the present study, results from previous afterglow plasma experiments were previously interpreted without taking into account the role of the buffer gas and, as a result, those experiments seemed to disagree with the storage ring experiments and with theoretical calculation. The present work reconciles observation data from the plasma and storage ring experiments and the theoretical result.

The obtained binary rate coefficient at 300 K is $\alpha_{\text{Bin}} = (4.7 \pm 1.5) \times 10^{-8} \text{ cm}^3 \text{ s}^{-1}$. The observed ternary recombination ($K_{\text{He}}(300 \text{ K}) = (2.5 \pm 1.2) \times 10^{-25} \text{ cm}^6 \text{ s}^{-1}$) is fast and at pressures of hundreds of Pa it is already dominant over the binary process. The dependence of the measured ternary recombination rate coefficient on temperature has a maximum at ~ 130 – 170 K. The observed ternary process is more effective by factor about 100 than the process of ternary recombination described by Bates and Khare [20].

To explain the process of fast ternary recombination we have developed a theoretical model for the process. In particular, we have calculated the delay time in $\text{H}_3^+ + e^-$ collisions (Δt as introduced by Smith [60]). We found that the delay time is sensitive to the rotational and nuclear-spin states of the H_3^+ ion. The delay time at collision energies $E \sim 150 \text{ cm}^{-1}$ can be of order of 100 ps for para- H_3^+ . During that collision time, the H_3^+ molecule ($\text{H}_3^+ + e^-$ complex) can collide with a helium atom, which enhances the overall plasma neutralization. The calculated delay time was used to derive the ternary recombination rate coefficient. The derived ternary coefficient as a function of temperature is smaller than the experimental value by a factor of order 2–10, which is plausible agreement for such a sophisticated process (from a theoretical *ab initio* point of view) within the somewhat heuristic theoretical method employed. Theory can in principle be further improved. In particular, the coefficient for l -changing collisions can be evaluated more accurately. At temperatures below 130 K there is a qualitative difference between measured and calculated values of the ternary rate coefficient: the experimental rate constant decreases with temperature, the theoretical one continues to grow. It is possible that at low temperature ortho and para- H_3^+ ion are not in thermal equilibrium in this afterglow plasma because of the very different binary rate constants $\alpha_{\text{Bin}}(T)$ that have been predicted for low temperatures. Nevertheless, for a first semiquantitative study of this kind, the agreement between theory and experiment for the ternary rate coefficients is encouraging.

Acknowledgments

This work is a part of the research plan MSM 0021620834 financed by the Ministry of Education of the Czech Republic and was partly supported by GACR (202/07/0495, 205/09/1183, 202/09/0642, 202/08/H057) by GAUK 53607, GAUK 124707 and GAUK 86908. It has also benefitted from support from the National Science Foundation, Grants Nos. PHY-0427460 and PHY-0427376, and from an allocation of NERSC supercomputing resources.

[1] T. Oka, Philos. Trans. R. Soc. London, Ser. A **364**, 2847 (2006).

[2] T. Geballe and T. Oka, Science **312**, 1610 (2006).

- [3] R. Plašil, J. Glosík, V. Poterya, P. Kudrna, J. Ruzs, M. Tichý, and A. Pysanenko, *Int. J. Mass Spectrom.* **218**, 105 (2002).
- [4] R. Johnsen, *J. Phys.: Conf. Ser.* **4**, 83 (2005).
- [5] M. Larsson and A. Orel, *Dissociative Recombination of Molecular Ions* (Cambridge University Press, Cambridge, 2008).
- [6] V. Kokoouline, C. Greene, and B. Esry, *Nature* **412**, 891 (2001).
- [7] V. Kokoouline and C. H. Greene, *Phys. Rev. A* **68**, 012703 (2003).
- [8] S. dos Santos, V. Kokoouline, and C. Greene, *J. Chem. Phys.* **127**, 124309 (2007).
- [9] C. Jungen and S. T. Pratt, *Phys. Rev. Lett.* **102**, 023201 (pages 4) (2009).
- [10] H. Kreckel, M. Motsch, J. Mikosch, J. Glosík, R. Plašil, S. Altevogt, V. Andrianarijaona, H. Buhr, J. Hoffmann, L. Lammich, et al., *Phys. Rev. Lett.* **95**, 263201 (2005).
- [11] B. J. McCall, A. J. Huneycutt, R. J. Saykally, T. R. Geballe, N. Djuric, G. H. Dunn, J. Semaniak, O. Novotny, A. Al-Khalili, A. Ehlerding, et al., *Nature* **422**, 500 (2003).
- [12] J. Glosík, R. Plašil, V. Poterya, P. Kudrna, and M. Tichý, *Chem. Phys. Lett* **331** (2000).
- [13] J. Glosík, R. Plasil, V. Poterya, P. Kudrna, M. Tichý, and A. Pysanenko, *J. Phys. B: At. Mol. Opt. Phys* **34**, L485 (2001).
- [14] T. Amano, *J. Chem. Phys* **92**, 6492 (1990).
- [15] T. Gougousi, R. Johnsen, and M. F. Golde, *Int. J. Mass Spectrom.* **149-150**, 131 (1995).
- [16] D. Smith and P. Španěl, *Int. J. Mass Spectrom.* **129**, 163 (1993).
- [17] V. Poterya, J. Glosík, R. Plašil, M. Tichý, P. Kudrna, and A. Pysanenko, *Phys. Rev. Lett.* **88**, 044802 (2002).
- [18] M. Larsson, B. McCall, and A. Orel, *Chem. Phys. Lett.* **462**, 145 (2008).
- [19] M. Fehér, A. Rohrbacher, and J. P. Maier, *Chem. Phys.* **185**, 357 (1994).
- [20] D. Bates and S. Khare, *Proc. Phys. Soc.* **85**, 231 (1965).
- [21] Y. Cao and R. Johnsen, *J. Chem. Phys.* **94**, 5443 (1991).
- [22] G. Goussset, B. Sayer, and J. Berlande, *Phys. Rev. A* **16**, 1070 (1977).
- [23] J. Glosík, I. Korolov, R. Plasil, O. Novotny, T. Kotrik, P. Hlavenka, J. Varju, I. A. Mikhailov, V. Kokoouline, and C. H. Greene, *J. Phys. B: At. Mol. Phys.* **41**, 191001 (2008).
- [24] J. Glosík, O. Novotný, A. Pysanenko, P. Zakouril, R. Plašil, P. Kudrna, and V. Poterya, *Plasma Sources Sci. Technol.* **12**, S117 (2003).
- [25] P. Macko, G. Bánó, P. Hlavenka, R. Plašil, V. Poterya, A. Pysanenko, O. Votava, R. Johnsen, and J. Glosík, *Int. J. Mass Spectrom.* **233**, 299 (2004).
- [26] P. Macko, G. Bánó, P. Hlavenka, R. Plašil, V. Poterya, A. Pysanenko, K. Dryahina, O. Votava, and J. Glosík, *Acta Phys. Slovaca* **54**, 263 (2004).
- [27] P. Kudrna, R. Plasil, J. Glosík, M. Tichy, V. Poterya, and J. Ruzs, *Czech. J. Phys.* **50**, 329 (2000).
- [28] R. Johnsen and J. Mitchell, *Advance in Gas-Phase Ion Chemistry*, vol. 3 (Elsevier, 1998).
- [29] N. Adams, D. Smith, and E. Alge, *J. Chem. Phys* **81**, 1778 (1984).
- [30] P. Macko, R. Plasil, P. Kudrna, P. Hlavenka, V. Poterya, A. Pysanenko, G. Bano, and J. Glosík, *Czech. J. Phys.* **52**, 695 (2002).
- [31] D. Strasser, L. Lammich, H. Kreckel, S. Krohn, M. Lange, A. Naaman, D. Schwalm, A. Wolf, and D. Zajfman, *Phys. Rev. A* **66**, 032719 (2002).
- [32] N. Adams, V. Poterya, and L. Babcock, *Mass Spectrom. Rev.* **25**, 798 (2006).
- [33] J. Glosík, P. Hlavenka, R. Plasil, F. Windisch, D. Gerlich, A. Wolf, and H. Kreckel, *Philos. Trans. R. Soc. A-Math. Phys. Eng. Sci.* **364**, 2931 (2006).
- [34] I. Korolov, R. Plasil, T. Kotrik, P. Dohnal, O. Novotny, and J. Glosík, *Contrib. Plasma Phys.* **48**, 461 (2008).
- [35] D. Trunec, P. Španěl, and D. Smith, *Chem. Phys. Lett.* **372**, 728 (2003).
- [36] M. Cordonnier, D. Uy, R. Dickson, K. Kerr, Y. Zhang, and T. Oka, *J. Chem. Phys.* **113**, 3181 (2000).
- [37] D. Gerlich, F. Windisch, P. Hlavenka, R. Plašil, and J. Glosík, *Philos. Trans. R. Soc. London, Ser. A* **364**, 3007 (2006).
- [38] L. Pagani, C. Vastel, E. Hugo, V. Kokoouline, C. Greene, A. Bacmann, E. Bayet, C. Ceccarelli, R. Peng, and S. Schlemmer, *Astron. Astrophys.* **494**, 623 (2009).
- [39] P. Atkins, *Physical Chemistry* (Oxford University Press, 1988).
- [40] D. Gerlich and S. Horning, *Chem. Rev.* **92**, 1509 (1992).
- [41] A. Florescu-Mitchell and J. Mitchell, *Phys. Rep.* **430**, 277 (2006).
- [42] J. Swift and M. Schwar, *Electrical Probes for Plasma Diagnostics* (Ilfie, London, 1970).
- [43] R. Plasil, I. Korolov, T. Kotrik, P. Dohnal, G. Bano, Z. Donko, and J. Glosík, *Eur. Phys. J. D* (2009), in print.
- [44] I. Korolov, T. Kotrik, R. Plasil, J. Varju, M. Hejduk, and J. Glosík, *Contrib. Plasma Phys.* **48**, 521 (2008).
- [45] E. McDaniel, J. Mitchell, and M. Rudd, *Atomic collisions, heavy Particles Projectiles* (John Wiley & Sons, New York, 1993).
- [46] M. Skrzypkowski, R. Johnsen, R. Rosati, and M. Golde, *Chem. Phys.* **296**, 23 (2004).
- [47] O. Pysanenko, O. Novotny, P. Zakouril, R. Plasil, V. Poterya, and J. Glosík, *Czech. J. Phys.* **52**, 681 (2002).
- [48] J. Glosík, R. Plasil, A. Pysanenko, O. Novotny, P. Hlavenka, P. Macko, and G. Bano, *J. Phys.: Conf. Ser.* **4**, 104 (2005).
- [49] S. Laubé, A. Le Padellec, O. Sidko, C. Rebrion-Rowe, J. Mitchell, and B. Rowe, *J. Phys. B: At. Mol. Opt. Phys.* **31**, 2111 (1998).
- [50] O. Novotny, R. Plasil, A. Pysanenko, I. Korolov, and J. Glosík, *J. Phys. B-At. Mol. Opt. Phys.* **39**, 2561 (2006).
- [51] M. Leu, M. Biondi, and R. Johnsen, *Phys. Rev. A* **8**, 413 (1973).
- [52] K. Hiraoka and P. Kebarle, *J. Chem. Phys.* **62**, 2267 (1975).
- [53] R. Plasil, P. Hlavenka, P. Macko, G. Bánó, A. Pysanenko, and J. Glosík, *J. Phys.: Conf. Ser.* **4**, 118 (2005).
- [54] I. Korolov, R. Plasil, T. Kotrik, P. Dohnal, and J. Glosík, *Int. J. Mass Spectrom.* **280**, 144 (2009).
- [55] B. McCall, A. Huneycutt, R. Saykally, N. Djuric, G. Dunn, J. Semaniak, O. Novotny, A. Al-Khalili, A. Ehlerding, F. Hellberg, et al., *Phys. Rev. A* **70**, 052716 (2004).
- [56] N. Adams and D. Smith, *Reactions of Small Transient Species* (Academic Press, New York, 1983).
- [57] J. Glosík, P. Zakouril, V. Hanzal, and V. Skalsky, *Int. J. Mass Spectrom. Ion Process.* **150**, 187 (1995).
- [58] J. Glosík, G. Bano, E. Ferguson, and W. Lindinger, *Int. J. Mass Spectrom.* **176**, 177 (1998).

- [59] I. Mistrík, R. Reichle, U. Müller, H. Helm, M. Jungen, and J. A. Stephens, Phys. Rev. A **61**, 033410 (2000).
- [60] F. T. Smith, Phys. Rev. **118**, 349 (1960).
- [61] A. P. Hickman, Phys. Rev. A **18**, 1339 (1978).